

PAPER • OPEN ACCESS

Theoretical studies of the THz compression of low-to-medium energy electron pulses and the single-shot stamping of electron–THz timing jitter

To cite this article: Yingpeng Qi *et al* 2021 *New J. Phys.* **23** 063052

View the [article online](#) for updates and enhancements.

You may also like

- [Tailoring terahertz radiation by controlling tunnel photoionization events in gases](#)
I Babushkin, S Skupin, A Husakou et al.
- [Active tunable THz metamaterial array implemented in CMOS technology](#)
Yongshan Liu, Tong Sun, Yong Xu et al.
- [Photonic terahertz technology](#)
Alvydas Lisauskas, Torsten Löffler and Hartmut G Roskos



PAPER

Theoretical studies of the THz compression of low-to-medium energy electron pulses and the single-shot stamping of electron-THz timing jitter

Yingpeng Qi^{1,6,*} , Lele Yang^{1,6}, Luye Yue¹, Jingjun Li¹, Xuan Wang^{2,3}, Zhenrong Sun⁴ and Jianming Cao^{1,5,*}¹ Center for Ultrafast Science and Technology, School of Physics and Astronomy, Shanghai Jiao Tong University, 200240 Shanghai, People's Republic of China² Beijing National Laboratory for Condensed Matter Physics, Institute of Physics, Chinese Academy of Sciences, Beijing 100190, People's Republic of China³ Songshan Lake Materials Laboratory, Dongguan, 523808, People's Republic of China⁴ State Key Laboratory of Precision Spectroscopy, East China Normal University, Shanghai 200062, People's Republic of China⁵ Physics Department and National High Magnetic Field Laboratory, Florida State University, Florida 32310, United States of America

* Authors to whom any correspondence should be addressed.

⁶ These authors contributed equally.E-mail: qiyp@sjtu.edu.cn and jcao@magnet.fsu.edu**Keywords:** low energy electron diffraction, electron-THz timing jitter, Coulomb interaction, attosecond temporal resolution, THz compressionRECEIVED
11 February 2021REVISED
26 May 2021ACCEPTED FOR PUBLICATION
27 May 2021PUBLISHED
17 June 2021Original content from
this work may be used
under the terms of the
[Creative Commons
Attribution 4.0 licence](https://creativecommons.org/licenses/by/4.0/).Any further distribution
of this work must
maintain attribution to
the author(s) and the
title of the work, journal
citation and DOI.

Abstract

The recent development of optical control of electron pulses brings new opportunities and methodologies in the fields of light–electron interaction and ultrafast electron diffraction (UED)/microscopy. Here, by a comprehensive theoretical study, we present a scheme to compress the longitudinal duration of low (≤ 1 keV) to medium energy (1–70 keV) electron pulses by the electric field of a THz wave, together with a novel shot-by-shot jitter correction approach by using the magnetic field from the same wave. Our theoretical simulations suggest the compression of the electron pulse duration to a few femtoseconds and even sub-femtosecond. A comprehensive analysis based on typical UED patterns indicates a sub-femtosecond precision of the jitter correction approach. We stress that the energy independence of Coulomb interaction in the compression and the compact structure of THz device lay the foundation of the compression of low energy electron pulses. The combination of the THz compression of the electron pulse and the electron-THz jitter correction opens a way to improve the overall temporal resolution to attosecond for ultrafast electron probes with low to medium energies and high charge number per pulse, and therefore, it will boost the ultrafast detection of transient structural dynamics in surface science and atomically thin film systems.

1. Introduction

Tailoring the properties of free electron pulses with THz and optical fields has sparked broad interest recently in the fields of shaping free-electron quantum states [1, 2], electron acceleration [3–10], and ultrafast electron diffraction (UED)/microscopy [11–17]. Compared to the widely used radiofrequency (RF) techniques, THz and optical field can reach much higher field strength and therefore, be more compact in space, as demonstrated in the dielectric laser accelerator [5–8] and the THz accelerator [3, 4]. For UED/microscopy, the most significant advantage of using THz/optical field to control free electron pulses is the much lower timing jitter between the driving field and the electron pulses, in contrast to RF techniques [18–24]. The peak-to-peak timing jitter is usually on the order of 10 fs for the THz field [11, 25] and attoseconds for the optical field [14], while the typical jitter for the RF field is ~ 50 fs [22, 26]. Recently, by using optical field to compress single-electron pulses, the attosecond synchronization and the attosecond electron pulse trains are achieved, which enables an overall attosecond temporal resolution for

UED/microscopy [1, 14, 15, 27]. However, to probe ultrafast structural/electronic dynamics which are irreversible or require a low repetition rate of pumping [28–33], isolated ultrashort electron pulses with high charge number are needed. To compress such a pulse, the half wavelength of the compression electric field must be longer than the pre-compressed pulse length, and a uniform field distribution over the transverse size of the electron pulse (typically 100 to 200 μm) is required. In this regard, THz field with a medium size wavelength between the optical and the RF field, is more suitable [3, 11]. However, for the THz compression of electron pulses, the synchronization jitter on the order of 10 fs still impedes achieving an attosecond temporal resolution and more work need to be done to solve this issue.

So far, most work focuses on compressing electron pulses with energies ranging from tens of keV to several MeV [1, 3, 11–17], while the compression of lower energy electron pulses has not been studied yet. In the community of UED, the interest in the low to medium energy UED with electronic kinetic energy of a few 100 eV to a few keV, has dramatically increased recently. The nano-tip [34, 35] or flat photocathode [36–38] based low to medium energy UED has been demonstrated, in which, a temporal resolution of tens to hundreds of femtoseconds has been achieved by lowering the electron number in a single pulse and shortening the propagation distance between the photocathode and the sample. Due to the large scattering cross section and the high damage threshold to samples, using low energy electron pulses as probes is beneficial for studying structural dynamics in atomically thin films [39] on surface [40, 41], such as the transient processes in the twistrionics [42–45] and the high temperature exciton condensation states [46, 47]. Further improving the temporal resolution without sacrificing the electron number of the low energy electron pulse is the key for these UEDs to apply to broader research fields.

In this work, we present a comprehensive theoretical study of the THz compression of low (≤ 1 keV) and medium energy (1–70 keV) electron pulses with a moderate charge number (10^3 – 10^5 electrons per pulse). The simulation results show that the compressed pulses can reach a few femtoseconds to sub-femtosecond pulse duration. In addition, we propose a novel approach to stamp the electron–THz timing jitter shot-by-shot, by simultaneously recording the modulation of a reference electron pulse by the magnetic field from the same THz pulse used for compression. A sub-fs accuracy of this jitter stamping approach is demonstrated by a comprehensive analysis based on some typical UED diffraction patterns. Our results demonstrate the potential to improve the overall temporal resolution to attosecond for ultrafast electron probes with low to medium electron energies, providing new opportunities in a broad range of researches on ultrafast structural dynamics.

2. Schemes for the THz compression of low to medium energy electron pulses and the electron–THz timing jitter correction

Before a quantitative analysis, we firstly discuss the three physical foundations for the THz compression of the low to medium energy electron pulses with a moderate charge number per pulse. First, we evaluate the impact of Coulomb interaction (CI) in the compression of low energy electron pulses. In our previous work, we propose the energy independence of CI in electron pulse compression [48]. The relativistic effect diminishes the Coulomb force F_c as $F_c \propto \beta^{-2}\gamma^{-3}$ (see page 296 in reference [49]), where β is the average velocity of electrons and γ is relativistic Lorentz factor, so low energy electron pulses will suffer stronger Coulomb repulsion force during the compression. However, the temporal focal length s is proportional to the kinetic energy of electron pulses as $s \propto \beta^2\gamma^3$ [48]. Then, the CI which integrates Coulomb force within the temporal focal length, i.e. $\text{CI} = \int_0^s F_c dz$, is energy-independent. In other words, the eV electron pulses suffer the same amount of CI as that of MeV electron pulses in the compression process. This energy independence of CI indicates that the compressed low to medium energy electron pulses hold the same beam quality as that of the conventional compressed 100 keV and MeV electron pulses. Second, the temporal focal length s for low to medium energy electron pulses is on the scale of a few millimeters to sub-millimeter, much shorter than that of high energy electron pulses (centimeters to meters). And therefore, a more compact millimeter-size compression device, shorter than s , is required [50, 51]. The recent developed ultra-compact THz devices can fulfill this requirement [3, 4, 52, 53]. Third, the impact of CI on diffraction pattern in the post-specimen region can be neglected in UED systems with a compression unit. Because the enlarged energy chirp by the compression field will extend the electron pulse duration very quickly after the temporal focus, quenching the CI induced distortion in diffraction patterns [54] to a negligible level.

The schematic of a UED system with our proposed THz compression unit is shown in figure 1(a). One femtosecond laser pulse is split into three pulses to generate photoelectron pulses, few-cycle THz pulses and to excite the sample as pump, respectively. The photoelectron pulses, including one probe pulse and one reference pulse, are accelerated by a DC field to a kinetic energy of 0.5–70 keV, and then interact with a THz standing field. The device housing such THz field is based on a recently demonstrated parallel-plate

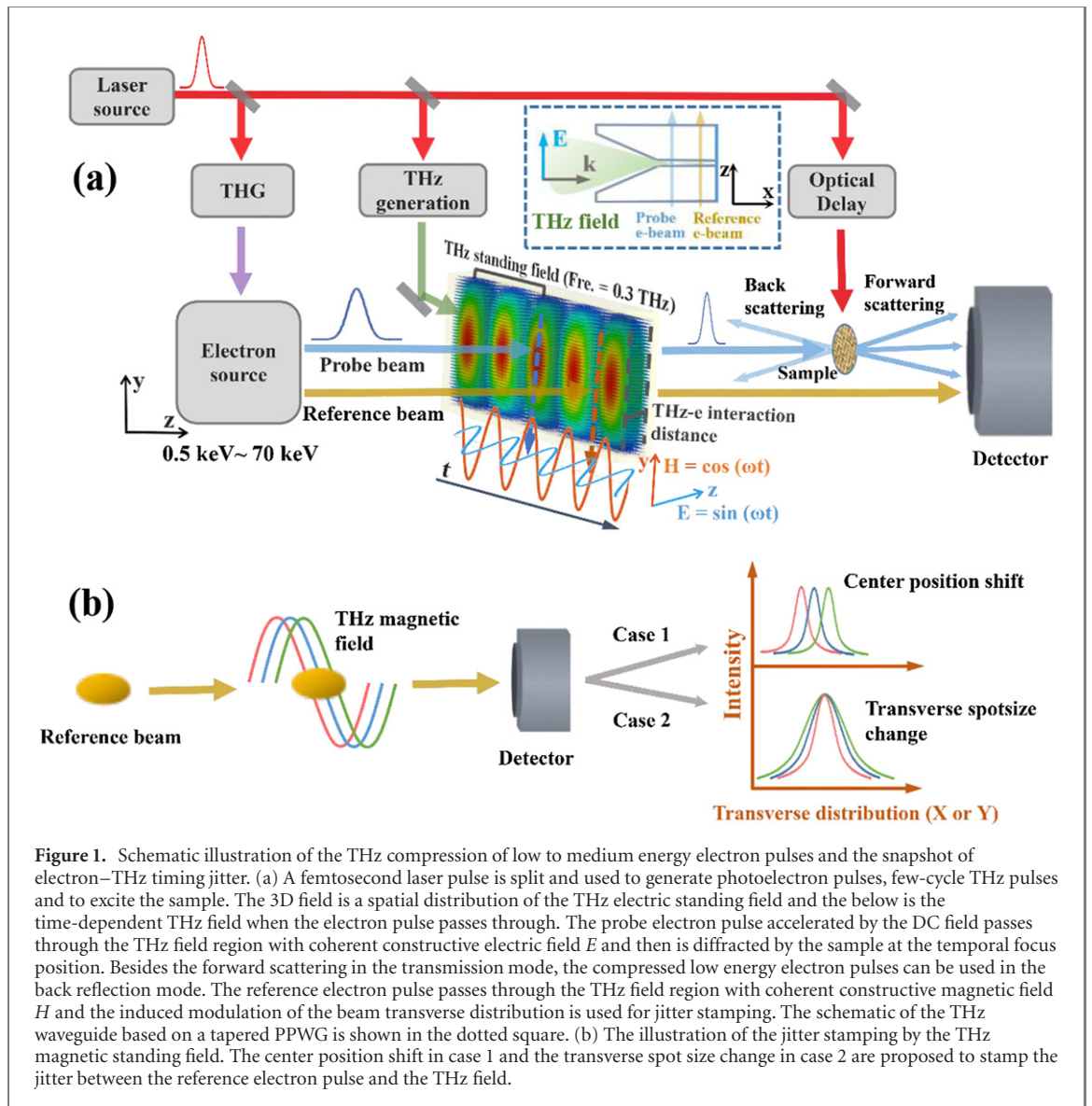


Figure 1. Schematic illustration of the THz compression of low to medium energy electron pulses and the snapshot of electron-THz timing jitter. (a) A femtosecond laser pulse is split and used to generate photoelectron pulses, few-cycle THz pulses and to excite the sample. The 3D field is a spatial distribution of the THz electric standing field and the below is the time-dependent THz field when the electron pulse passes through. The probe electron pulse accelerated by the DC field passes through the THz field region with coherent constructive electric field E and then is diffracted by the sample at the temporal focus position. Besides the forward scattering in the transmission mode, the compressed low energy electron pulses can be used in the back reflection mode. The reference electron pulse passes through the THz field region with coherent constructive magnetic field H and the induced modulation of the beam transverse distribution is used for jitter stamping. The schematic of the THz waveguide based on a tapered PPWG is shown in the dotted square. (b) The illustration of the jitter stamping by the THz magnetic standing field. The center position shift in case 1 and the transverse spot size change in case 2 are proposed to stamp the jitter between the reference electron pulse and the THz field.

waveguide (PPWG) structure (or horn structure) [12, 52, 55, 56] which can produce standing electric and magnetic waves with an intrinsic $\pi/2$ phase difference between them (note that the phase difference does not need to be exact $\pi/2$ for the subsequent simulation and design). The schematic of a tapered PPWG structure that can focus THz pulses and give rise to a uniform field distribution across the gap is shown in figure 1(a). In the simulation, a continuous THz standing field with a central frequency of 0.3 THz is generated between two parallel plates by CST studio (see appendix A for the 3D structure of the parallel plates), mimicking the uniform field distribution across the gap in such a PPWG [52]. The impact of the entrance and the exit aperture on the plates for electron pulses passing through, is negligible to the compression (see appendix A for the simulation results). For an experimental implementation, the tunable single-cycle or multicycle narrowband THz field used in the simulations can be generated by existing methods [11, 17, 57, 58]. As shown in figure 1(a), the probe electron pulse passes through the position of the parallel plates with coherent constructive THz electric field (i.e. the antinode position) at the zero crossing phase (indicated by the dashed blue arrow), imprinting an energy chirp on the probe beam for the subsequent pulse compression. The compressed electron pulse can work either in the transmission mode for low to medium energy electron pulse to study atomically thin and thicker films, or in the reflection mode for low energy electron pulse to study ultrafast surface dynamics. The propagation and the compression of electron pulses are simulated by general particle tracer (GPT) with a 3D space charge model [59]. The 3D THz field, as shown in figure 1(a), is generated by CST studio and imported into GPT to simulate the THz control of electron pulses. In order for an easy experimental implementation, no magnetic lens is used in this THz compression based UED system, similar to those compact UED designs [37, 60, 61]. And the beam qualities are still good enough to give decent diffraction patterns in such a design (see appendix B for more details).

To reach a sub-femtosecond temporal resolution, both the pulse duration and the jitter correction need to be on the sub-femtosecond timescale. The microscale suppression of the CI [48] limits the minimum achievable compressed pulse duration, so a feasible solution is to lower the electron number to a level of 10^3 – 10^4 per pulse. However, lowering electron number degenerates the accuracy of most shot-by-shot jitter stamping approaches, such as methods proposed in references [16, 48, 62], due to inadequate signal-to-noise ratio. Here, we propose a novel jitter correction approach to remove this restriction and gain a higher jitter stamping accuracy. As shown in figure 1(a), a reference electron pulse passes through the position of the parallel plates with coherent constructive (or destructive) THz magnetic field at the zero crossing phase (indicated by the dashed orange arrow), then the transverse distribution of the reference pulse is modulated due to the timing jitter between the reference pulse and the THz magnetic field. Since the probe and reference electron pulses are derived from the same laser pulse, this timing jitter for the reference pulse equals the timing jitter for the probe pulse. A schematic illustration of the jitter stamping approach is shown in figure 1(b). The spatial modulation of the reference pulse in transverse direction can be either the center position shift in case 1 or the transverse spot size change in case 2 (see more details on the magnetic field distribution and the spatial modulation regime in appendix A). The combination of the probe pulse compression and the jitter stamping by the reference pulse provides a feasible way toward sub-femtosecond temporal resolution. In contrast to the recent studies using THz streaking to stamp the jitter between the RF field and the electron pulses in MeV UED [16, 17], the jitter correction approach in this work stamps the intrinsic jitter between the THz compression field and the electron pulses. Moreover, the spatial separation of the probe pulse and the reference pulse indicates that this jitter correction approach is noninvasive without disturbing the diffraction patterns.

3. Simulations for the THz compression of low to medium energy electron pulses

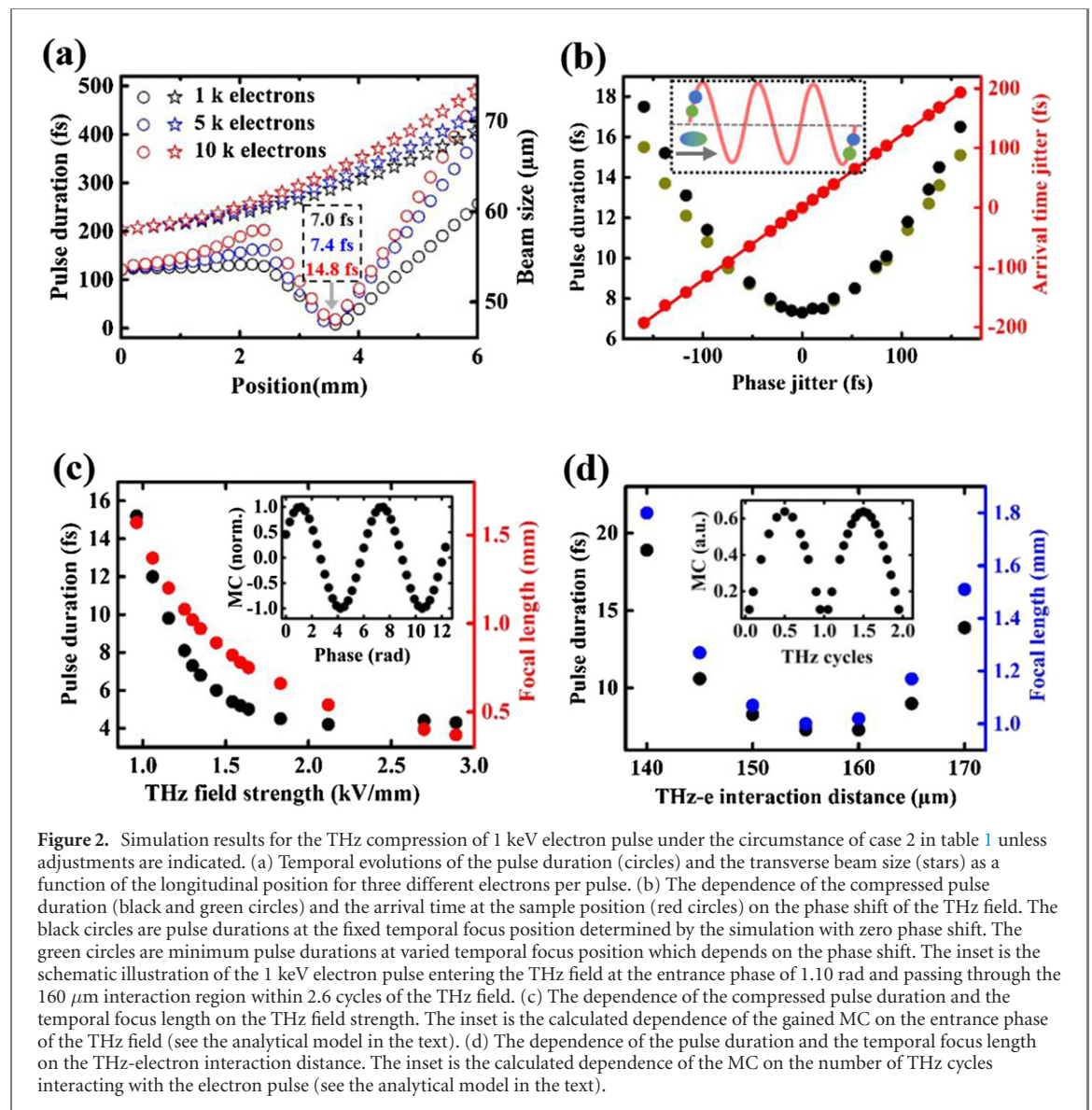
Simulation results for the THz compression of electron pulses with 0.5 keV, 1 keV, 2 keV, 5 keV and 70 keV kinetic energies are summarized as five cases in table 1. The initial parameters of electron pulses and the THz fields in the simulation are chosen from the commonly used or readily accessible values in the UED community. Electron distributions of compressed and uncompressed electron pulses are shown in the appendix C. Note that the simulation results listed in table 1 aim at convenient experimental implementation, and more details about the compression regime and compression results on specific experimental requirements are discussed in subsequent figures 2 and 3.

In the case of the compression of 1 keV electron pulse, i.e. case 2 in table 1, the temporal evolution of the electron pulse duration and the transverse spot size are displayed in figure 2(a). The electron pulse is compressed to ~ 10 fs by the THz field with a field strength of ~ 1.0 kV mm^{-1} , while the transverse spot size expands continuously which indicates that the transverse divergence is not impacted by the longitudinal compression. The dependence of the compressed pulse duration on the phase jitter of the THz field is shown in figure 2(b). The peak-to-peak jitter of the THz field is on the order of tens of femtoseconds [11, 25], and such jitter changes the compressed pulse duration in less than 1 fs, which is much smaller than the few femtoseconds pulse duration and therefore can be neglected. The linear ratio between the phase shift of the THz field and the arrival time change (i.e. the red spots) of electron pulses at the sample position is 1.22 as shown in figure 2(b), indicating that the CI during compression is dynamically suppressed similar as that in the compression of high energy electron pulses [20]. The inset in figure 2(b) displays the schematic of the interaction between the THz electric field and the electron pulse. The 1 keV electron pulse enters the THz field at the entrance phase of 1.10 rad and passes through the 160 μm interaction region (see table 1) within 2.6 THz cycles. The interaction of low energy electron pulses with multicycle THz fields aims to lengthen the interaction region to a few 100 microns, a size easier for the THz waveguide to be fabricated with conventional machining techniques [12, 52]. The compression scheme is the same as that in the compression of high energy electron pulses, i.e. the tails electrons gain more energy than the head electrons from the compression field then catch up the head electrons at the temporal focus. By increasing the THz field strength, both the pulse duration and the temporal focus length are decreased as shown in figure 2(c). A balance between the compressed pulse duration and the temporal focus length is needed preventing a too short temporal focus for a practical experimental implementation. In this work, a temporal focus length no less than 1 mm is designed for an easy experimental implementation [37, 60]. The minimum pulse duration in figure 2(c) is around 4 fs rms. A further compression is possible by breaking the limit from the microscale suppression of the CI [48] and the high order nonlinear term of the compression field [63], which is beyond the scope of this work. The impact of the entrance and exit apertures on the THz device to the compression is examined and no significant impact is observed as shown in the appendix A.

The inset in figure 2(c) shows a sinusoidal modulation of the momentum chirp (MC) of an electron pulse by the phase of the THz field. The momentum changes of the head and tail electrons (i.e. Δp_{head} and

Table 1. Initial parameters and simulation results for the THz compression of low to medium energy electron pulses.

Parameters	Case 1	Case 2	Case 3	Case 4	Case 5
Electron pulse energy	0.5 keV	1 keV	2 keV	5 keV	70 keV
Initial pulse duration (RMS)	15 fs	15 fs	15 fs	15 fs	15 fs
Initial beam radius (RMS)	58 μm	58 μm	58 μm	66 μm	58 μm
Initial energy spread	0.1 eV	0.1 eV	0.1 eV	0.1 eV	0.1 eV
Electrons per pulse	1 k	5 k	10 k	10 k	50 k
Accelerating field strength	1.25 kV mm ⁻¹	2.5 kV mm ⁻¹	2.0 kV mm ⁻¹	2.5 kV mm ⁻¹	7.0 kV mm ⁻¹
Pulse duration before compression (RMS)	270 fs	167 fs	183 fs	158 fs	120 fs
Beam radius before compression	62 μm	61 μm	61 μm	70 μm	70 μm
Energy spread before compression	0.048%	0.12%	0.08%	0.078%	0.12%
Distance from photocathode to THz field	2.4 mm	2.4 mm	3 mm	5 mm	20 mm
THz frequency	0.3 THz	0.3 THz	0.3 THz	0.3 THz	0.3 THz
THz-e interaction distance	150 μm	160 μm	150 μm	200 μm	200 μm
THz field strength	0.6 kV mm ⁻¹	1.3 kV mm ⁻¹	1.4 kV mm ⁻¹	1.9 kV mm ⁻¹	9.6 kV mm ⁻¹
Compressed electron pulse duration (RMS)	17.1 fs	7.4 fs	8.6 fs	5.0 fs	3.7 fs
Temporal focal length	1.10 mm	1.06 mm	2.28 mm	3.70 mm	14.9 mm
Transverse spot size (RMS) at temporal focus	67 μm	63 μm	65 μm	74 μm	66 μm
Energy spread after compression	0.46%	0.70%	0.66%	0.40%	0.47%
Divergence after compression	8.40 mrad	6.78 mrad	4.79 mrad	1.61 mrad	0.96 mrad



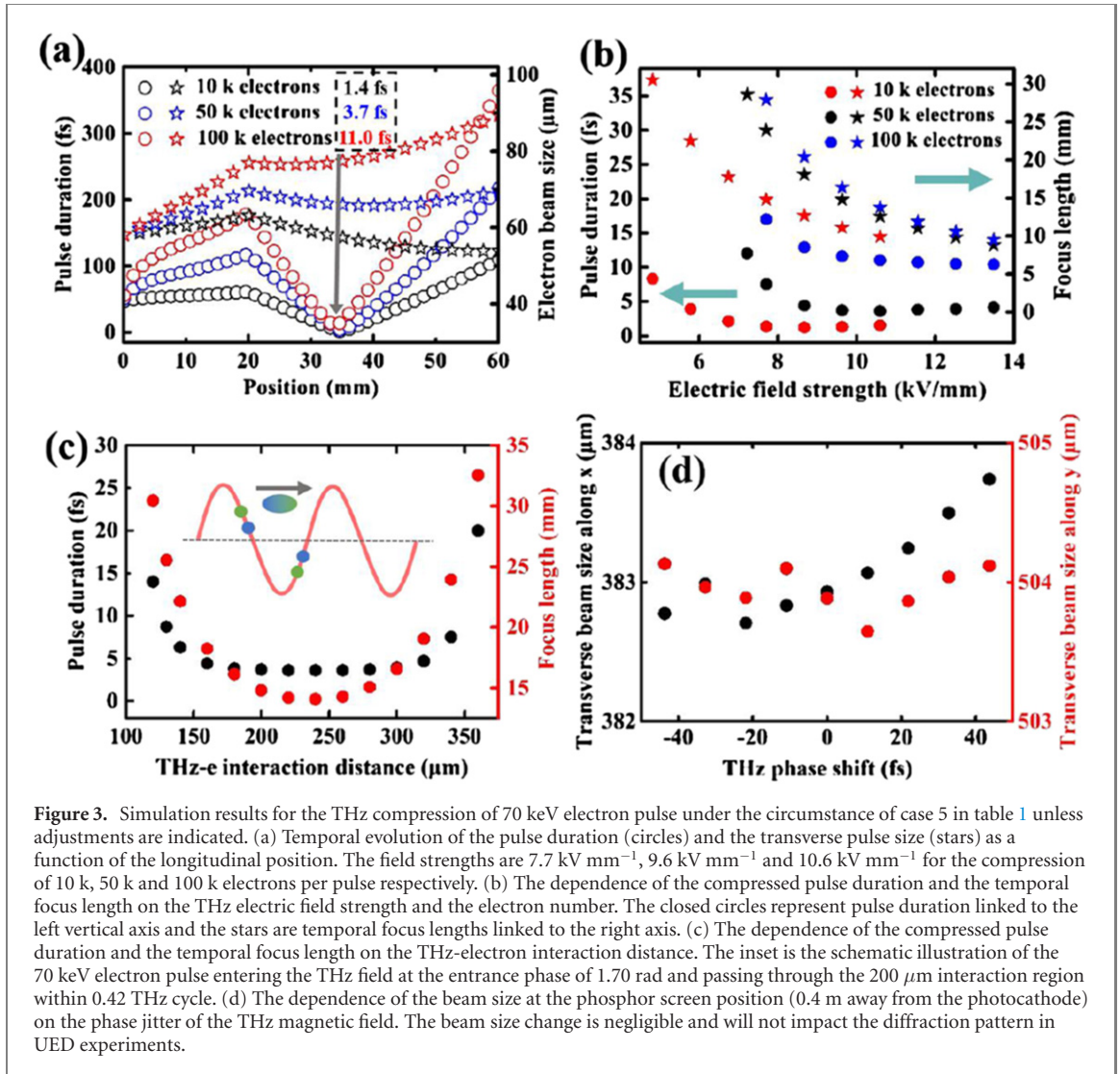


Figure 3. Simulation results for the THz compression of 70 keV electron pulse under the circumstance of case 5 in table 1 unless adjustments are indicated. (a) Temporal evolution of the pulse duration (circles) and the transverse pulse size (stars) as a function of the longitudinal position. The field strengths are 7.7 kV mm^{-1} , 9.6 kV mm^{-1} and 10.6 kV mm^{-1} for the compression of 10 k, 50 k and 100 k electrons per pulse respectively. (b) The dependence of the compressed pulse duration and the temporal focus length on the THz electric field strength and the electron number. The closed circles represent pulse duration linked to the left vertical axis and the stars are temporal focus lengths linked to the right axis. (c) The dependence of the compressed pulse duration and the temporal focus length on the THz-electron interaction distance. The inset is the schematic illustration of the 70 keV electron pulse entering the THz field at the entrance phase of 1.70 rad and passing through the 200 μm interaction region within 0.42 THz cycle. (d) The dependence of the beam size at the phosphor screen position (0.4 m away from the photocathode) on the phase jitter of the THz magnetic field. The beam size change is negligible and will not impact the diffraction pattern in UED experiments.

Δp_{tail}) gain from the THz field can be estimated as:

$$\Delta p_{\text{head}} = e * A * \int_0^{t_{\text{E-THz}}} \sin(\omega t + \varphi) dt \quad (1)$$

$$\Delta p_{\text{tail}} = e * A * \int_{t_{\text{dur}}}^{t_{\text{E-THz}} + t_{\text{dur}}} \sin(\omega t + \varphi) dt, \quad (2)$$

where e is the electronic charge of the electron, A is the amplitude of the THz field, t_{dur} is the duration of the electron pulse before compression, $t_{\text{E-THz}}$ is the timescale of the electron pulse passing through the THz field, φ is the phase of THz field when electron beam enters. Then the overall MC gained from the THz field is $\Delta p = \Delta p_{\text{head}} - \Delta p_{\text{tail}}$. The phase of ~ 1.0 rad in the analytical model for maximal MC in the inset of figure 2(c) coincides with the optimized entrance phase of 1.10 rad for maximal pulse compression obtained in the simulation. Based on this analytical model, the inset in figure 2(d) displays the modulation of the MC by changing the THz field cycles interacting with electron pulses. In order to compress the electron pulse, the head electrons will be slowed down and the tail electrons will be speeded up after interacting with the THz field, then generally half of the period of the THz field is used for achieving a maximum energy chirp [18, 20, 21]. However, the short wavelength of the THz field enables a lengthened interaction period by adding an integer cycle. As demonstrated in the inset of figure 2(d), the 0.5 THz cycle, 1.5 THz cycle, 2.5 THz cycle give the same maximal energy chirp and therefore the same compression ratio. Note that the speed of the low energy electron pulse ($< 1 \text{ keV}$) is $< 1.8 \times 10^7 \text{ m s}^{-1}$, much smaller than the speed of the THz field. If the low energy electron pulse interacts with 0.5 (2.5) THz cycle, the THz-electron interaction distance is $\sim 30 \mu\text{m}$ ($\sim 160 \mu\text{m}$). In this case, to lower the difficulty in fabricating waveguides, we choose the 2.6 THz cycle to perform simulations with GPT. The pulse duration and the temporal focus length as a function of the THz-electron interaction distance, are shown in figure 2(d). The compressed

pulse duration is found to be very sensitive to the interaction distance between the THz field and the electron pulse, so a calculation of the required MC based on the above presented analytical model is necessary before an experimental design and implementation.

The ultra-compact structure and the cost efficiency of the THz waveguide in comparing with conventional RF technique makes the THz field an excellent alternative in compression of medium to high energy electron pulses. In figure 3, we present the simulation results for the compression of 70 keV electron pulses. The minimum pulse duration of 1.4 fs (rms) with 1×10^4 electrons in single pulse is obtained as shown in figure 3(a). Further compression reaching a sub-fs duration is achievable by further decreasing the electron number and optimizing the electron–THz interaction. Note that, concomitant with the longitudinal compression, the THz magnetic field gives rise to a focusing of the transverse pulse size as shown in figure 3(a). Though the magnetic field is coherently destructive at the position where the electric field is coherently constructive, the small wavelength of the THz field and the velocity dependent Lorentz force make the 70 keV electrons feel the magnetic field. In order to examine the impact of the transverse focusing on the diffraction pattern, we simulate the dependence of the pulse size at the phosphor screen position (0.4 m away from the photocathode) on the phase jitter of the THz magnetic field, and the results are summarized in figure 3(d). The $\sim 0.5 \mu\text{m}$ transverse spot size change within ± 40 fs phase jitter suggests a negligible impact of the phase jitter on the peak intensity of diffraction spots/rings in UED experiments. The dependence of the compressed pulse duration and the temporal focus length on the THz electric field strength and the electron numbers are shown in figure 3(b). The temporal focus length is roughly 10–20 mm and readily accessible for the experimental implementation. The compressed pulse duration and the temporal focus length as a function of the THz–electron interaction distance are shown in figure 3(c). The inset in figure 3(c) displays the schematic of the interaction between the THz electric field and the electron pulse. The 70 keV electron pulse enters the THz field at the entrance phase of 1.70 rad and passes through the 200 μm interaction region (see table 1) within 0.42 THz cycles.

4. Single-shot stamping of the electron–THz timing jitter

To achieve a sub-fs temporal resolution in the THz compression based UED/microscopy, the timing jitter between the electron pulse and the THz field must be stamped and corrected shot by shot. Here we propose a novel approach, as depicted in figure 1(b), to stamp the electron–THz timing jitter. If no jitter, the reference pulse will pass through the THz magnetic field at the phase crossing the zero, suffering no modulation in the beam position and the transverse spot size. However, the THz phase jitter will shift the passing through phase and modulate the transverse spot size and the transverse center position of the reference pulse (see appendix A for more detailed information). Thus, by tracking these two parameter changes of the reference beam, the corresponding electron–THz timing jitter can be determined.

Specifically, this novel approach can be carried out in two ways: either tracing the beam size change or monitoring the beam position change. We examined the feasibility and accuracy of these two methods by a combination of simulations and analyzing experimental diffraction patterns. The subsequent simulations are based on the compression condition in case 5 in table 1. The schematic in figure 4(a) is the jitter stamping by recording the transverse spot size change of the reference pulse induced by the THz magnetic field. The accuracy in measuring the spot size change of the reference pulse is determined through fitting the FWHM of the (200) reflection in static diffraction patterns of MoTe_2 using a Gaussian function. More information about the experimental system can be found elsewhere [60]. As shown in figure 4(a), the accuracy of the fit over 20 images is 0.09 pixels, i.e. 1.4 μm (15.6 μm per pixel of the detector), which is nearly the same as the allowed detection of spot width change in reference [11]. A cosinusoidal modulation of the transverse spot size of the reference pulse generated by tuning the phase of the THz magnetic field is displayed in figure 4(b) (left). The spot size change is characterized at a position of 0.4 m away from the THz field. The linear part, marked by a dotted ellipse, is used for the jitter stamping. The linear change of the transverse spot size on the phase jitter of the THz magnetic field is shown in figure 4(b) (right). The linear ratio in combination with the accuracy in fitting the spot size in figure 4(a) suggests a precision of 1.77 fs for the field strength of 10.5 kV mm^{-1} and 0.83 fs for the field strength of 21.0 kV mm^{-1} in stamping the jitter. The precision can be further improved by enlarging the spot size change, such as lengthening the distance between the THz field and the phosphor screen.

Note that the above method aims at stamping the jitter shot-by-shot, however, the pulse-to-pulse electron number change can also contribute to the spot size change and degenerate the precision of the jitter stamping. As shown in the appendix D, the linear ratio of $\sim 0.8 \mu\text{m fs}^{-1}$ retains as the electron number changes, whereas the absolute spot size changes $\sim 24 \mu\text{m}$ with every 10% change of the electron number. Fortunately, the electron number change can be corrected by counting the intensity change of the beam at the phosphor screen, therefore, the electron number fluctuation induced degeneration can be monitored

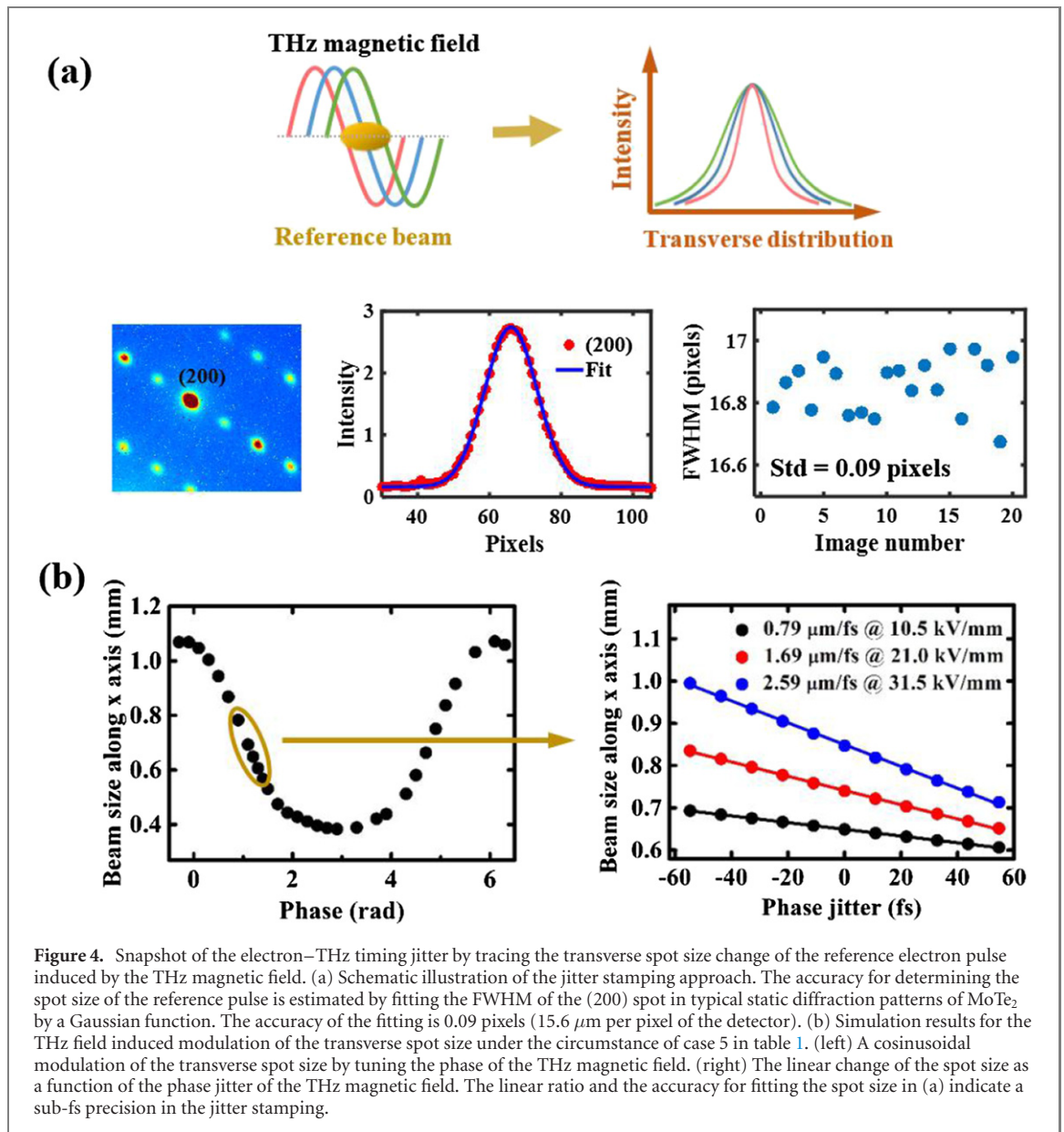


Figure 4. Snapshot of the electron–THz timing jitter by tracing the transverse spot size change of the reference electron pulse induced by the THz magnetic field. (a) Schematic illustration of the jitter stamping approach. The accuracy for determining the spot size of the reference pulse is estimated by fitting the FWHM of the (200) spot in typical static diffraction patterns of MoTe₂ by a Gaussian function. The accuracy of the fitting is 0.09 pixels (15.6 μm per pixel of the detector). (b) Simulation results for the THz field induced modulation of the transverse spot size under the circumstance of case 5 in table 1. (left) A cosinusoidal modulation of the transverse spot size by tuning the phase of the THz magnetic field. (right) The linear change of the spot size as a function of the phase jitter of the THz magnetic field. The linear ratio and the accuracy for fitting the spot size in (a) indicate a sub-fs precision in the jitter stamping.

and corrected. In order to evaluate the detectable electron number change, we measure the intensity fluctuation of the brightest spot (200) in single crystalline diffraction patterns of MoTe₂, as shown in the appendix E. The measured peak-to-peak intensity fluctuation is $\sim 0.2\%$, i.e. the upper limit of the electron number change can be measured in experiments is 0.2% . Then the measurable electron spot size change induced by electron number fluctuation is $\sim 0.5 \mu\text{m}$. Based on the linear ratio of $0.79 \mu\text{m fs}^{-1}$ in figure 4(b), the degeneration of the jitter stamping precision by the electron number fluctuation can be suppressed to sub-fs. In table 2 in the appendix D, the ratio of the spot size change to the phase jitter is retained as the electron number increases, so much more electrons in the reference pulse can be used to further improve the signal-to-noise ratio and the precision of the jitter stamping.

The schematic for the snapshot of timing jitter by recording the center position shift of the reference beam is shown in figure 5(a). The cosinusoidal modulation of the center position of the reference pulse induced by tuning the phase of the THz magnetic field is shown in figure 5(b) (top right). The position calculating the center position shift is 0.4 m away from the THz field position. The linear part marked by a dotted ellipse is used for the jitter stamping. The linear change of the center position on the phase jitter in the range of ± 60 fs is shown in figure 5(b) (bottom). The electron pulse pointing instability will degenerate the precision in measuring the center position shift. In UED experimental system, the electron pulse pointing instability is $\sim 10 \mu\text{m}$ in the single pulse regime [16, 62, 64] and $1.56 \mu\text{m}$ in accumulation regime [11]. The linear ratio in figure 5(b) (bottom right) in combination with the pointing instability implies a precision of 1.66 fs (with the THz field strength of 21.0 kV mm^{-1}) in the single shot mode and 0.26 fs (with the THz field strength of 21.0 kV mm^{-1}) in the accumulation mode in stamping the jitter. The electron

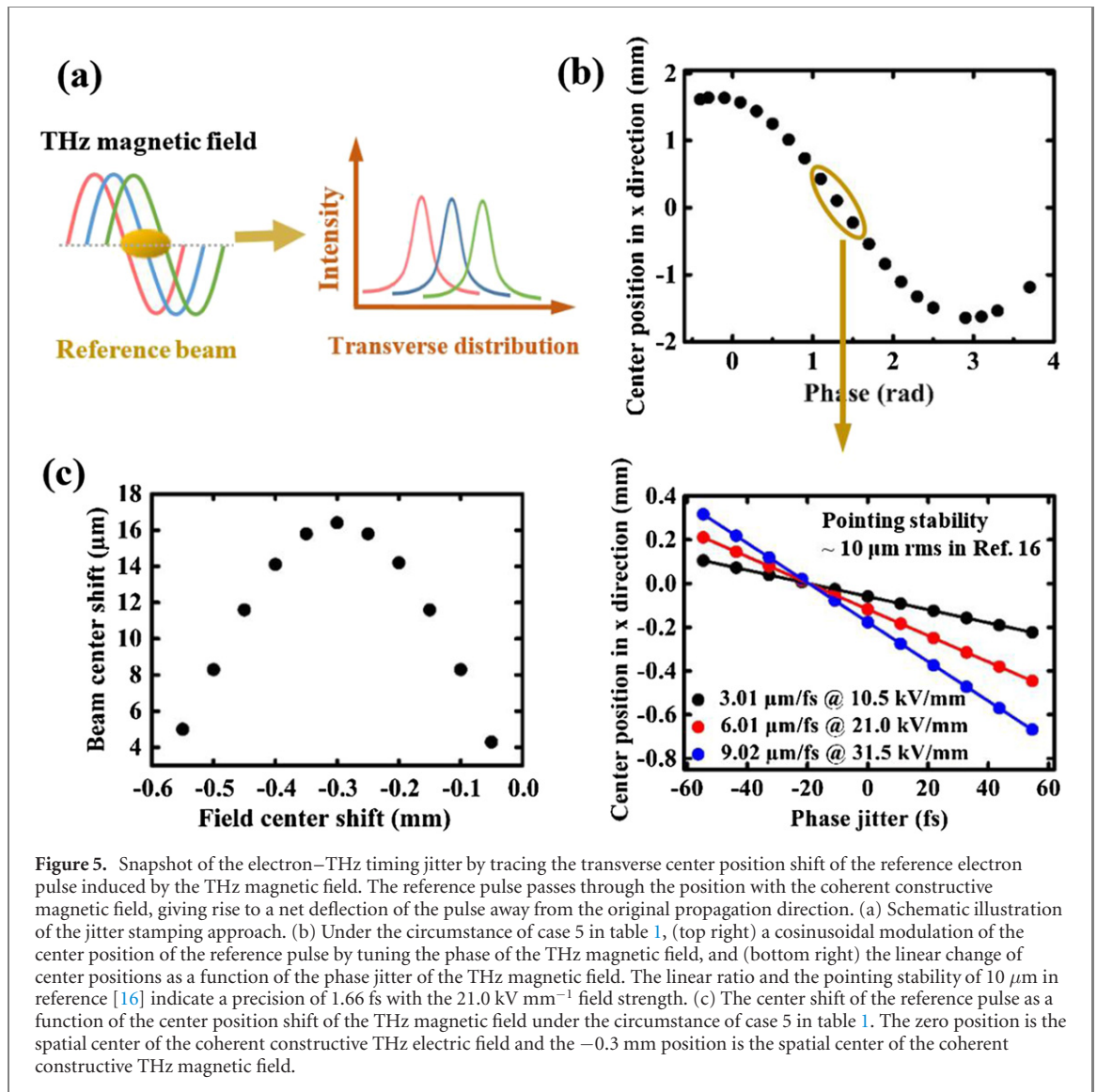


Figure 5. Snapshot of the electron–THz timing jitter by tracing the transverse center position shift of the reference electron pulse induced by the THz magnetic field. The reference pulse passes through the position with the coherent constructive magnetic field, giving rise to a net deflection of the pulse away from the original propagation direction. (a) Schematic illustration of the jitter stamping approach. (b) Under the circumstance of case 5 in table 1, (top right) a cosinusoidal modulation of the center position of the reference pulse by tuning the phase of the THz magnetic field, and (bottom right) the linear change of center positions as a function of the phase jitter of the THz magnetic field. The linear ratio and the pointing stability of $10 \mu\text{m}$ in reference [16] indicate a precision of 1.66 fs with the 21.0 kV mm^{-1} field strength. (c) The center shift of the reference pulse as a function of the center position shift of the THz magnetic field under the circumstance of case 5 in table 1. The zero position is the spatial center of the coherent constructive THz electric field and the -0.3 mm position is the spatial center of the coherent constructive THz magnetic field.

pulse center shift as a function of the center position change of the THz magnetic field is shown in figure 5(c), which indicates that a well alignment of the reference beam passing through the spatial center of the magnetic field is required for a high precision jitter stamping. Lengthening the distance between the THz field and the phosphor screen will decrease the impact of the beam pointing instability and further improve the precision of the jitter stamping to sub-fs.

5. Conclusions

In this work, we present a comprehensive theoretical study of the electron pulse compression by the THz field, extending to low beam energy region which is not regularly accessed by the conventional RF technique. We discuss the physical foundation for the THz compression of low-to-medium energy electron pulses, and carry out precise numerical simulations and analytical analyses, which pave the way for the further experimental implementation. Our results show that for electron pulse with beam energy less than 1 keV and thousands of electrons per pulse, a sub-10 fs rms pulse duration can be routinely maintained. These results reaffirm our earlier finding of energy independence of CI [48], suggesting that the compressed low energy electron pulses hold the same beam quality as that of the compressed 100 keV and MeV electron pulses. For the THz compression of medium energy electron pulses, a minimum 1.4 fs rms pulse duration can be realized and even sub-fs pulse duration is achievable by reducing the number of electrons per pulse to below 10^4 . In addition, we propose a novel approach to stamp the THz-electron synchronization jitter on a shot by shot scheme and a sub-fs precision is determined through a comprehensive analysis on typical UED diffraction patterns. This jitter stamping approach is also applicable in UED and UEM experiments using optical field to control electron pulses. Our work shows an overall sub-fs temporal resolution of UED

with a compressed single pulse, which is comparable to that of attosecond pulse trains by optical field compression [1, 14]. Such compressed single pulse based UED with the electron number per pulse several orders of magnitude larger than that of attosecond pulse trains, is a more generic case in exploring laser–matter interaction.

Contributions

Yingpeng Qi devised the project and conceived the presented ideas. Lele Yang performed the numerical simulation under the supervision of Yingpeng Qi. Yingpeng Qi performed the theoretical analysis and collected the experimental data. The paper was written by Yingpeng Qi with contributions from all the authors.

Acknowledgments

Yingpeng Qi carried out the experiments on MoTe₂ with the help from Daniela Zahn, Thomas Vasileiadis, Hélène Seiler, Yoav William Windsor and Ralph Ernstorfer during his postdoc period at Fritz Haber Institute in Berlin. We acknowledge support from the Sino-German (CSC-DAAD) Postdoc Scholarship Program (Grant Nos. 201709920054 and 57343410), the funding from Max Plank Society, and the National Natural Science Foundation of China under Grant No. 11974241. Xuan Wang would like to acknowledge support from the National Natural Science Foundation of China under Grant No. 11774409.

Data availability

The data that support the findings of this study are available from the corresponding author upon reasonable request.

Appendix A. THz magnetic standing field in a THz device

See figure A.

Appendix B. The dependence of the scattering angle and the divergence of the free propagating electron pulse on the kinetic energy and the electron number per pulse

In the schematic of the THz compression of low to medium energy UED in figure 1(a) and subsequent simulations, no magnetic lens is used. Instead, a compact structure from electron source to the sample is taken for an easy experimental implementation, which is similar to the compact concept in conventional UED system [37, 60, 61]. High reciprocal space resolution or *s*-resolution is required in UED systems to identify the ring or spot features in diffraction patterns and track changes of their intensity, position, and width with high precision. With the electron number of 10^3 to 10^5 , the divergence of the free propagating electron pulse and the scattering angle reflected by the (111) plane of the aluminum film in the energy range of 0.5 keV–70 keV are show in figure B(a) in appendix B. In figure B(b), the ratio between the scattering angle and the divergence indicates that the divergence is smaller than the scattering angles by one order of magnitude, which is comparable to the beam quality in conventional keV and MeV UED [22]. Importantly, as demonstrated by subsequent simulation results in figures 2(a) and 3(a), the compression will not change the divergence of the electron pulse with a moderate charge number. So the compact design for the THz compression of low to medium energy in figure 1(a) is effective and reliable to keep high quality of diffraction patterns. A focusing lens after the sample can be placed to optimize the diffraction patterns [37, 60, 61] if needed. The compact design in compression based UED will improve the compression ability by suppressing the nonlinear curvature of the compression field [48, 63].

Appendix C. Propagation time of electrons in a single pulse at the positions before compression and at the temporal focus position

See figure C.

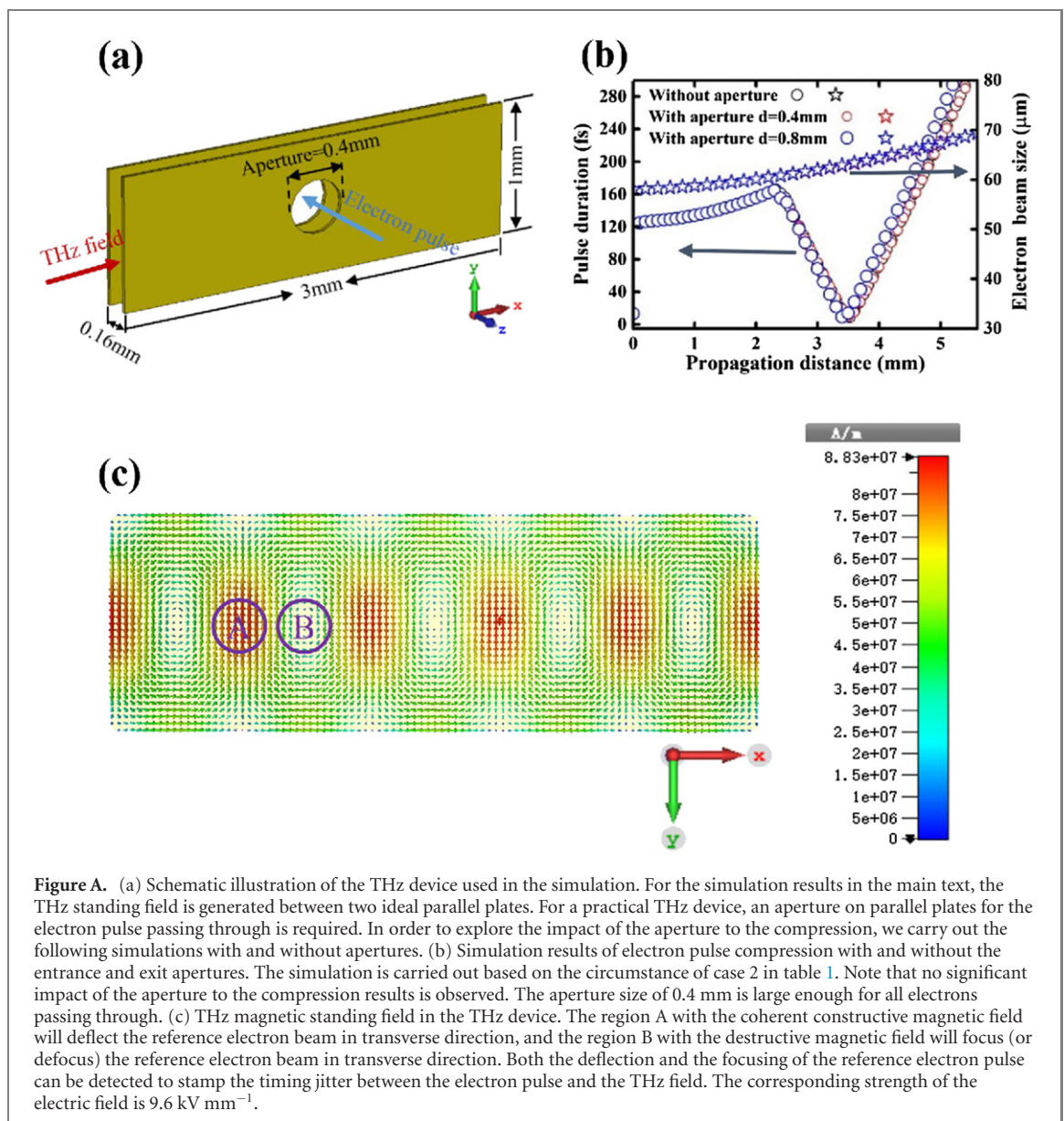


Figure A. (a) Schematic illustration of the THz device used in the simulation. For the simulation results in the main text, the THz standing field is generated between two ideal parallel plates. For a practical THz device, an aperture on parallel plates for the electron pulse passing through is required. In order to explore the impact of the aperture to the compression, we carry out the following simulations with and without apertures. (b) Simulation results of electron pulse compression with and without the entrance and exit apertures. The simulation is carried out based on the circumstance of case 2 in table 1. Note that no significant impact of the aperture to the compression results is observed. The aperture size of 0.4 mm is large enough for all electrons passing through. (c) THz magnetic standing field in the THz device. The region A with the coherent constructive magnetic field will deflect the reference electron beam in transverse direction, and the region B with the destructive magnetic field will focus (or defocus) the reference electron beam in transverse direction. Both the deflection and the focusing of the reference electron pulse can be detected to stamp the timing jitter between the electron pulse and the THz field. The corresponding strength of the electric field is 9.6 kV mm^{-1} .

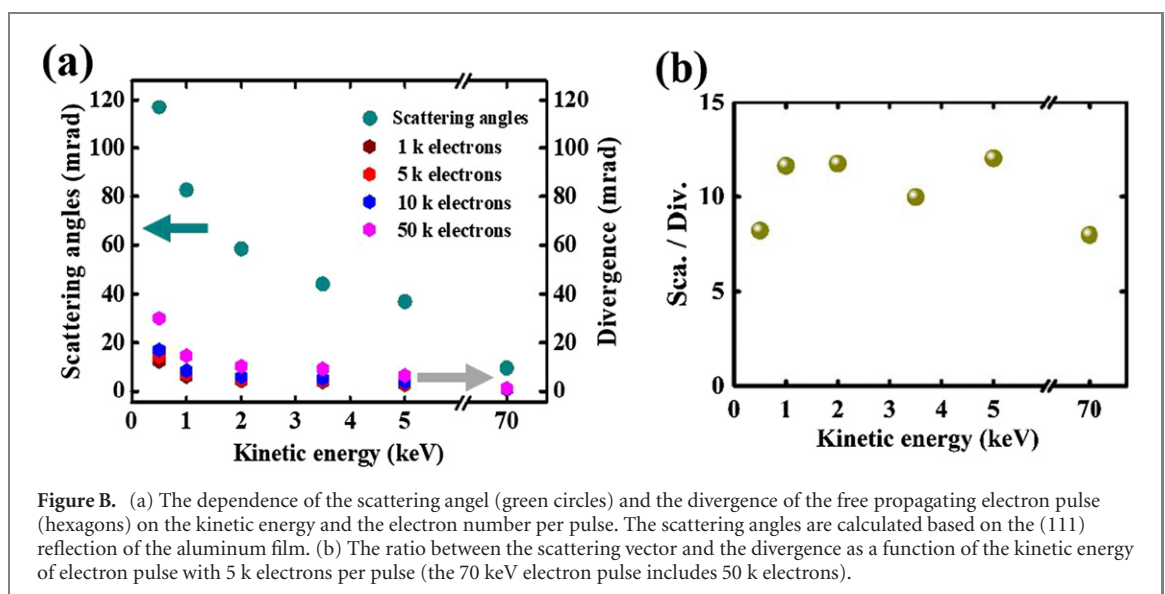
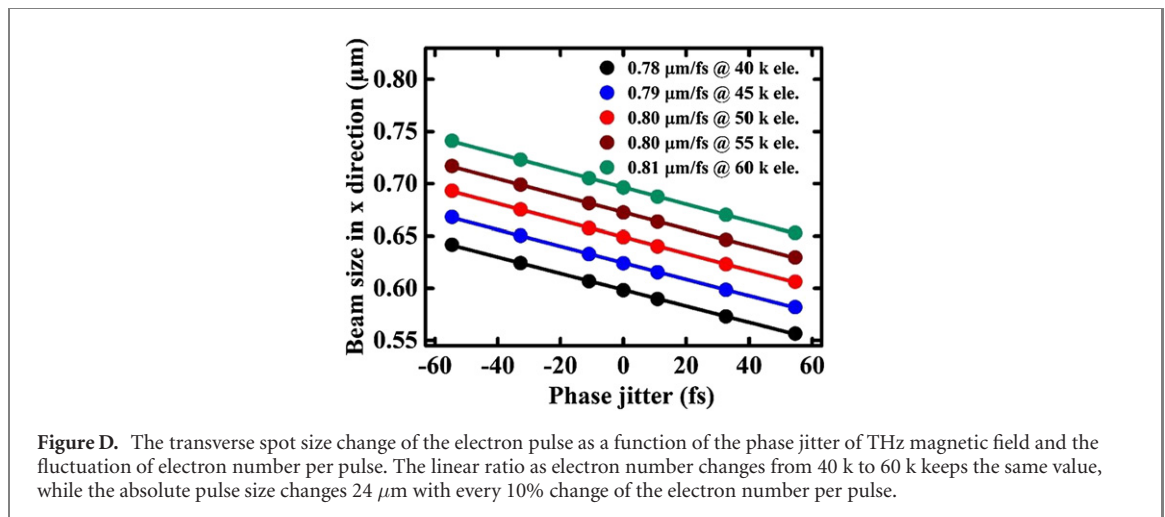
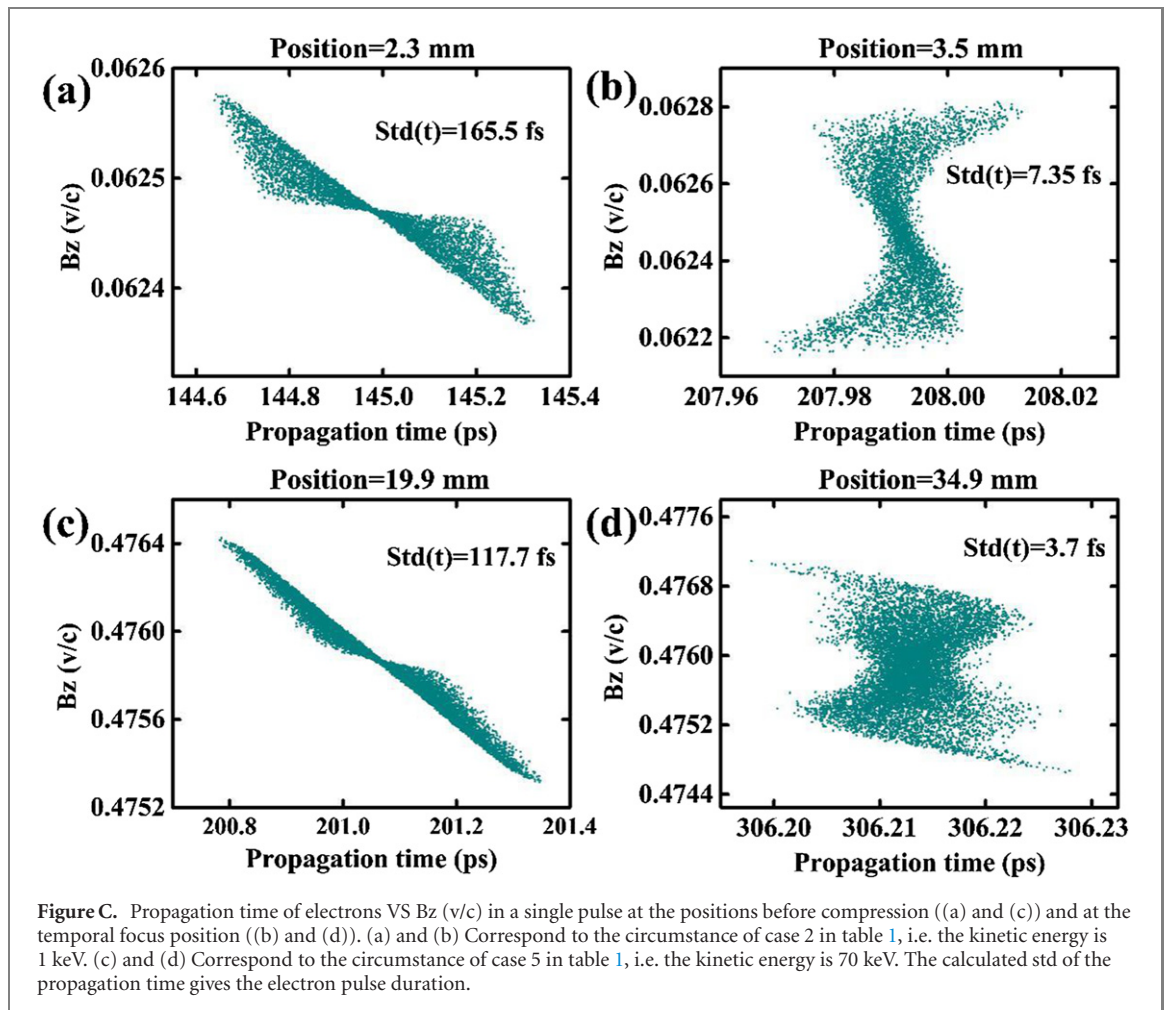


Figure B. (a) The dependence of the scattering angle (green circles) and the divergence of the free propagating electron pulse (hexagons) on the kinetic energy and the electron number per pulse. The scattering angles are calculated based on the (111) reflection of the aluminum film. (b) The ratio between the scattering vector and the divergence as a function of the kinetic energy of electron pulse with 5 k electrons per pulse (the 70 keV electron pulse includes 50 k electrons).



Appendix D. The dependence of the transverse spot size of the electron pulse on the phase jitter of THz magnetic field and the fluctuation of electron number per pulse

See figure D and table 2.

Appendix E. Evaluation of the detectable intensity change

See figure E.

Table 2. Dependence of the pulse size change on the number of electrons per pulse.

Number of electrons per pulse (k)	Pulse size change ($\mu\text{m fs}^{-1}$)
50	0.80
100	0.84
200	0.89
500	0.92

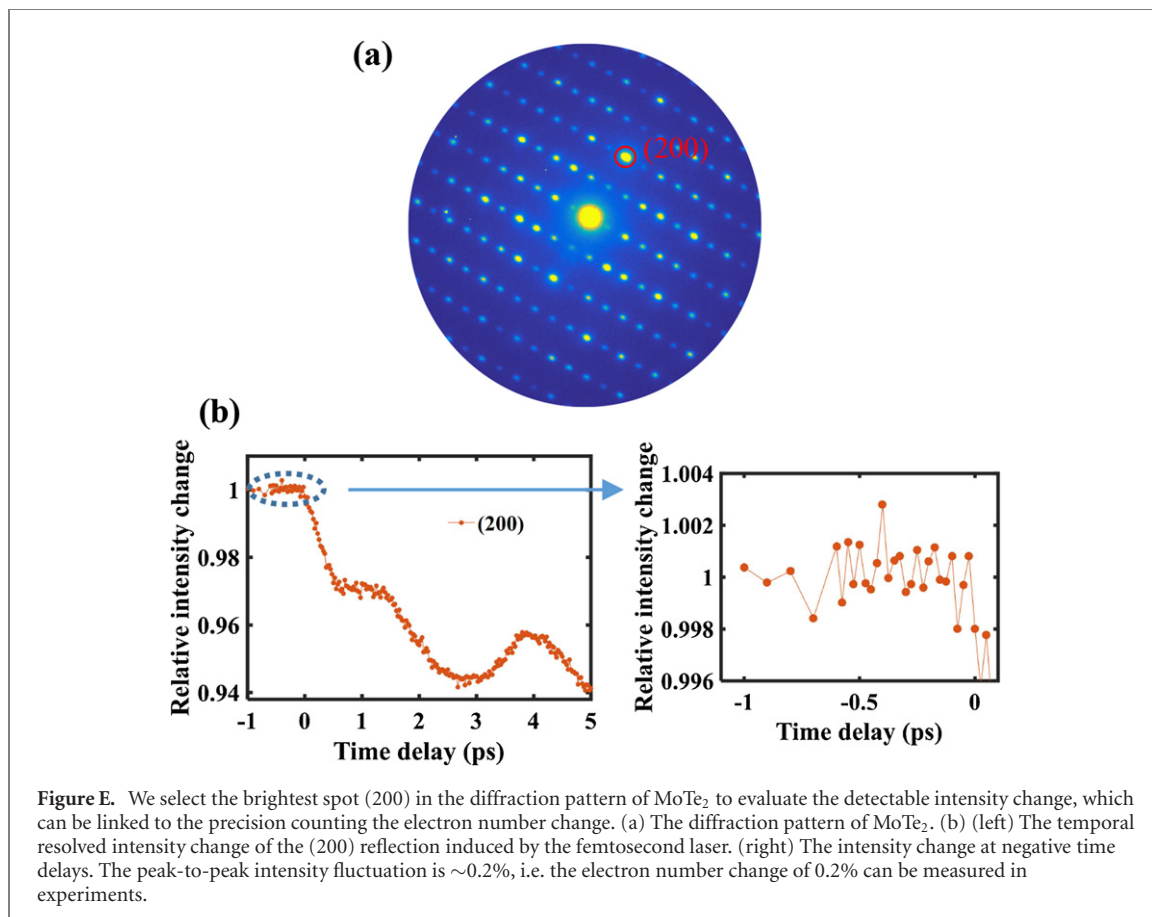


Figure E. We select the brightest spot (200) in the diffraction pattern of MoTe₂ to evaluate the detectable intensity change, which can be linked to the precision counting the electron number change. (a) The diffraction pattern of MoTe₂. (b) (left) The temporal resolved intensity change of the (200) reflection induced by the femtosecond laser. (right) The intensity change at negative time delays. The peak-to-peak intensity fluctuation is $\sim 0.2\%$, i.e. the electron number change of 0.2% can be measured in experiments.

ORCID iDs

Yingpeng Qi  <https://orcid.org/0000-0001-5950-8157>

References

- [1] Priebe K E, Rathje C, Yalunin S V, Hohage T, Feist A, Schäfer S and Ropers C 2017 Attosecond electron pulse trains and quantum state reconstruction in ultrafast transmission electron microscopy *Nat. Photon.* **11** 793
- [2] Dahan R *et al* 2020 Resonant phase-matching between a light wave and a free-electron wavefunction *Nat. Phys.* **16** 1123
- [3] Zhang D *et al* 2018 Segmented terahertz electron accelerator and manipulator (STEAM) *Nat. Photon.* **12** 336
- [4] Nanni E A, Huang W R, Hong K-H, Ravi K, Fallahi A, Moriena G, Dwayne Miller R J and Kärtner F X 2015 Terahertz-driven linear electron acceleration *Nat. Commun.* **6** 8486
- [5] Peralta E A *et al* 2013 Demonstration of electron acceleration in a laser-driven dielectric microstructure *Nature* **503** 91
- [6] Breuer J and Hommelhoff P 2013 Laser-based acceleration of nonrelativistic electrons at a dielectric structure *Phys. Rev. Lett.* **111** 134803
- [7] Schönenberger N, Mittelbach A, Yousefi P, McNeur J, Niedermayer U and Hommelhoff P 2019 Generation and characterization of attosecond microbunched electron pulse trains via dielectric laser acceleration *Phys. Rev. Lett.* **123** 264803
- [8] Black D S, Niedermayer U, Miao Y, Zhao Z, Solgaard O, Byer R L and Leedle K J 2019 Net acceleration and direct measurement of attosecond electron pulses in a silicon dielectric laser accelerator *Phys. Rev. Lett.* **123** 264802
- [9] Hebling J *et al* 2011 Optical manipulation of relativistic electron beams using THz pulses (arXiv:1109.6852)
- [10] Turnár S, Hebling J, Fülöp J A, Tóth G, Almási G and Tibai Z 2021 Design of a THz-driven compact relativistic electron source *Appl. Phys. B* **127** 38
- [11] Kealhofer C, Schneider W, Ehberger D, Ryabov A, Krausz F and Baum P 2016 All-optical control and metrology of electron pulses *Science* **352** 429

- [12] Snively E C *et al* 2020 Femtosecond compression dynamics and timing jitter suppression in a THz-driven electron bunch compressor *Phys. Rev. Lett.* **124** 054801
- [13] Zhao L *et al* 2020 Femtosecond relativistic electron beam with reduced timing jitter from THz driven beam compression *Phys. Rev. Lett.* **124** 054802
- [14] Morimoto Y and Baum P 2018 Diffraction and microscopy with attosecond electron pulse trains *Nat. Phys.* **14** 252
- [15] Ryabov A, Thurner J W, Nabben D, Tsarev M V and Baum P 2020 Attosecond metrology in a continuous-beam transmission electron microscope *Sci. Adv.* **6** eabb1393
- [16] Li R K *et al* 2019 Terahertz-based subfemtosecond metrology of relativistic electron beams *Phys. Rev. Accel. Beams* **22** 012803
- [17] Zhao L *et al* 2018 Terahertz streaking of few-femtosecond relativistic electron beams *Phys. Rev. X* **8** 021061
- [18] Van Oudheusden T, Pasmans P L E M, van der Geer S B, de Loos M J, van der Wiel M J and Luiten O J 2010 Compression of subrelativistic space-charge-dominated electron bunches for single-shot femtosecond electron diffraction *Phys. Rev. Lett.* **105** 264801
- [19] Pasmans P L E M, van den Ham G B, Dal Conte S F P, van der Geer S B and Luiten O J 2013 Microwave TM₀₁₀ cavities as versatile 4D electron optical elements *Ultramicroscopy* **127** 19
- [20] Qi Y, Pei M, Qi D, Li J, Yang Y, Jia T, Zhang S and Sun Z 2017 Coulomb interaction-induced jitter amplification in RF-compressed high-brightness electron source ultrafast electron diffraction *New J. Phys.* **19** 023015
- [21] Chatelain R P, Morrison V R, Godbout C and Siwick B J 2012 Ultrafast electron diffraction with radio-frequency compressed electron pulses *Appl. Phys. Lett.* **101** 081901
- [22] Weathersby S P *et al* 2015 Mega-electron-volt ultrafast electron diffraction at SLAC national accelerator laboratory *Rev. Sci. Instrum.* **86** 073702
- [23] Maxson J, Cesar D, Calmasini G, Ody A, Musumeci P and Alesini D 2017 Direct measurement of sub-10 fs relativistic electron beams with ultralow emittance *Phys. Rev. Lett.* **118** 154802
- [24] Gliserin A, Walbran M, Krausz F and Baum P 2015 Sub-phonon-period compression of electron pulses for atomic diffraction *Nat. Commun.* **6** 8723
- [25] Ehberger D, Mohler K J, Vasileiadis T, Ernstorfer R, Waldecker L and Baum P 2019 Terahertz compression of electron pulses at a planar mirror membrane *Phys. Rev. Appl.* **11** 024034
- [26] Otto M R, René de Cotret L P, Stern M J and Siwick B J 2017 Solving the jitter problem in microwave compressed ultrafast electron diffraction instruments: robust sub-50 fs cavity-laser phase stabilization *Struct. Dyn.* **4** 051101
- [27] Morimoto Y and Baum P 2020 Single-cycle optical control of beam electrons *Phys. Rev. Lett.* **125** 193202
- [28] Siwick B J, Dwyer J R, Jordan R E and Miller R J D 2003 An atomic-level view of melting using femtosecond electron diffraction *Science* **302** 1382
- [29] Mo M Z *et al* 2018 Heterogeneous to homogeneous melting transition visualized with ultrafast electron diffraction *Science* **360** 1451
- [30] Sciaini G *et al* 2009 Electronic acceleration of atomic motions and disordering in bismuth *Nature* **458** 56
- [31] Yang J *et al* 2018 Imaging CF₃I conical intersection and photodissociation dynamics with ultrafast electron diffraction *Science* **361** 64
- [32] Gao M *et al* 2013 Mapping molecular motions leading to charge delocalization with ultrabright electrons *Nature* **496** 343
- [33] Miller R J D 2014 Femtosecond crystallography with ultrabright electrons and x-rays: capturing chemistry in action *Science* **343** 1108
- [34] Storeck G, Vogelgesang S, Sivis M, Schäfer S and Ropers C 2017 Nanotip-based photoelectron microgun for ultrafast LEED *Struct. Dyn.* **4** 044024
- [35] Müller M, Paarmann A and Ernstorfer R 2014 Femtosecond electrons probing currents and atomic structure in nanomaterials *Nat. Commun.* **5** 5292
- [36] Karrer R, Neff H J, Hengsberger M, Greber T and Osterwalder J 2001 Design of a miniature picosecond low-energy electron gun for time-resolved scattering experiments *Rev. Sci. Instrum.* **72** 4404
- [37] Badali D S, Gengler R Y N and Miller R J D 2016 Ultrafast electron diffraction optimized for studying structural dynamics in thin films and monolayers *Struct. Dyn.* **3** 034302
- [38] Lee C, Kassier G and Miller R J D 2018 Optical fiber-driven low energy electron gun for ultrafast streak diffraction *Appl. Phys. Lett.* **113** 133502
- [39] Gulde M, Schweda S, Storeck G, Maiti M, Yu H K, Wodtke A M, Schafer S and Ropers C 2014 Ultrafast low-energy electron diffraction in transmission resolves polymer/graphene superstructure dynamics *Science* **345** 200
- [40] Lee J J *et al* 2014 Interfacial mode coupling as the origin of the enhancement of Tc in FeSe films on SrTiO₃ *Nature* **515** 245
- [41] Yuan W *et al* 2020 Visualizing H₂O molecules reacting at TiO₂ active sites with transmission electron microscopy *Science* **367** 428
- [42] Cao Y *et al* 2018 Correlated insulator behaviour at half-filling in magic-angle graphene superlattices *Nature* **556** 80
- [43] Cao Y, Fatemi V, Fang S, Watanabe K, Taniguchi T, Kaxiras E and Jarillo-Herrero P 2018 Unconventional superconductivity in magic-angle graphene superlattices *Nature* **556** 43
- [44] Regan E C *et al* 2020 Mott and generalized Wigner crystal states in WSe₂/WS₂ moiré superlattices *Nature* **579** 359
- [45] Seyler K L, Rivera P, Yu H, Wilson N P, Ray E L, Mandrus D G, Yan J, Yao W and Xu X 2019 Signatures of moiré-trapped valley excitons in MoSe₂/WSe₂ heterobilayers *Nature* **567** 66
- [46] Wang Z, Rhodes D A, Watanabe K, Taniguchi T, Hone J C, Shan J and Mak K F 2019 Evidence of high-temperature exciton condensation in two-dimensional atomic double layers *Nature* **574** 76
- [47] Varsano D, Palumbo M, Molinari E and Rontani M 2020 A monolayer transition-metal dichalcogenide as a topological excitonic insulator *Nat. Nanotechnol.* **15** 367
- [48] Qi Y, Yang Y, Sun H, Wang X, Cao J, Ernstorfer R and Sun Z 2020 Dynamical suppression of Coulomb interaction and sub-fs jitter correction in electron pulse compression *New J. Phys.* **22** 093004
- [49] Wangler T P R F 2008 *Linear Accelerators* 2nd edn (New York: Wiley)
- [50] Lassise A, Mutsaers P H A and Luiten O J 2012 Compact, low power radio frequency cavity for femtosecond electron microscopy *Rev. Sci. Instrum.* **83** 043705
- [51] Verhoeven W, van Rens J F M, Kemper A H, Rietman E H, van Doorn H A, Koole I, Kieft E R, Mutsaers P H A and Luiten O J 2019 Design and characterization of dielectric filled TM₁₁₀ microwave cavities for ultrafast electron microscopy *Rev. Sci. Instrum.* **90** 083703
- [52] Othman M A K, Hoffmann M C, Kozina M E, Wang X J, Li R K and Nanni E A 2019 Parallel-plate waveguides for terahertz-driven MeV electron bunch compression *Opt. Express* **27** 23791

- [53] Fallahi A and Kärtner F 2018 Design strategies for single-cycle ultrafast electron guns *J. Phys. B: At. Mol. Opt. Phys.* **51** 144001
- [54] Chatelain R P, Morrison V, Godbout C, van der Geer B, de Loos M and Siwick B J 2012 Space-charge effects in ultrafast electron diffraction patterns from single crystals *Ultramicroscopy* **116** 86
- [55] Vashchenko G et al 2018 Performance analysis of the prototype THz-driven electron gun for the AXSIS project *Nucl. Instrum. Methods Phys. Res. A* **909** 177
- [56] Kim S-H, Lee E S, Ji Y B and Jeon T-I 2010 Improvement of THz coupling using a tapered parallel-plate waveguide *Opt. Express* **18** 1289
- [57] Lu J, Hwang H Y, Li X, Lee S-H, Kwon O-P and Nelson K A 2015 Tunable multi-cycle THz generation in organic crystal HMQ-TMS *Opt. Express* **23** 22723
- [58] Ravi K, Schimpf D N and Kärtner F X 2016 Pulse sequences for efficient multi-cycle terahertz generation in periodically poled lithium niobate *Opt. Express* **24** 25582
- [59] Van der Geer S B and De Loos M J 2016 The general particle tracer code <http://pulsar.nl/gpt>
- [60] Waldecker L, Bertoni R and Ernstorfer R 2015 Compact femtosecond electron diffractometer with 100 keV electron bunches approaching the single-electron pulse duration limit *J. Appl. Phys.* **117** 044903
- [61] Gerbig C, Senfleben A, Morgenstern S, Sarpe C and Baumert T 2015 Spatio-temporal resolution studies on a highly compact ultrafast electron diffractometer *New J. Phys.* **17** 043050
- [62] Gao M, Jiang Y, Kassier G H and Dwayne Miller R J 2013 Single shot time stamping of ultrabright radio frequency compressed electron pulses *Appl. Phys. Lett.* **103** 033503
- [63] Floettmann K 2014 Generation of sub-fs electron beams at few-MeV energies *Nucl. Instrum. Methods Phys. Res. A* **740** 34
- [64] Yang X, Li J, Fedurin M, Smaluk V, Yu L, Wu L, Wan W, Zhu Y and Shaftan T 2019 A novel nondestructive diagnostic method for mega-electron-volt ultrafast electron diffraction *Sci. Rep.* **9** 17223